Lawrence Berkeley National Laboratory

Title
CRYOPUMP BEHAVIOR IN THE PRESENCE OF BEAM OR NUCLEAR RADIATION

Permalink
https://escholarship.org/uc/item/0d54w3jz

Author
Law, P.K.

Publication Date
1977-12-01

CRYOPUMP BEHAVIOR IN THE PRESENCE OF BEAM

OR NUCLEAR RADIATION

Peter K. Law

Lawrence Berkeley Laboratory
Berkeley, California 94720

CRYOPUMP BEHAVIOR IN THE PRESENCE OF BEAM OR

NUCLEAR RADIATION

Peter K. Law

Contents

ABSTRACT

Cryocondensation pumping has been proposed to be the method of gas removal for neutral-beam refueled fusion reactors. A cryo-condensation pumping unit has been constructed to test design concepts and compatibility with conditions under actual beam operation and nuclear radiation environment.

Various operating parameters for this test pumping unit have been measured, including pumping speeds for various gases and beam desorption effects.

An experiment has been planned at the Berkeley Research Reactor to measure the desorption effects of high energy neutrons and gamma radiation. A foil activation method has been devised to accurately assess the energy spectrum of this neutron source, which is expected to be comparable to that of the Tokamak Fusion Test Reactor.

I.   Introduction

The attainment and maintenance of high vacuum in a thermo-
nuclear fusion device is essential due to the existence of serious
energy-loss mechanisms that would otherwise occur. Many aspects
of the vacuum problem are being investigated, such as vacuum-wall
materials research,[1] desorption effects,[2] sublimation pumping,[3] and
better materials fabrication and prepararion methods.[4]

In parts further removed from the plasma, especially inside
neutral-beam injection ducts where very large gas-load removal is
required,[5] cryocondensation pumping will be the primary means of
gas and impurity removal. Cryopumping is the only choice for this
purpose because of its high pumping speed and almost total absence
of contamination, even given the chance of failure.[6] However, much
information about condensed gas behavior, design parameters, and
experience with operation under various conditions must be made
available before large cryopumps can be incorporated into a thermo-
nuclear fusion device.

A.   Impurity Effects in Fusion Reactor Operations

High atomic number impurities sputtered and blistered off
vacuum walls, and cold background gases from various sources, par-
ticularly neutral beam injectors, if not removed, would result in
driving up both the ignition condition and the Lawson criterion.

The energy-loss mechanisms include impurity-driven instabilities,[7] radiation emission,[8] and greater fuel requirements through more intense neutral beam injection and ohmic heating.

The ignition condition of a steady-state homogeneous D-T reactor is given by[9]

$$\frac{3}{2} \left(n_e kT_e + \sum_i n_i kT_i \right) = \left(\langle \sigma v \rangle \; U_\alpha n_D n_T - P_{rad} \right) \tau$$

where

$\langle \sigma v \rangle$ = D-T reaction rate average over a Maxwellian energy distribution

v_α = 3.52 MeV (assuming complete energy deposition in plasma by alpha particle)

fn_e = concentration of single impurity species of atomic number z which is fully ionized

and

P_{rad} = $R(f,z,T)n_e^2$ = radiated power, which includes free-free bremsstrahlung, recombination and line radiation.

Under these conditions, the ignition condition can be written as, assuming $T_e = T_i \simeq T$,

$$n_\ell \tau = \frac{\frac{3}{2} kT \left[1 + (1 - fz) + f \right]}{\frac{\langle \sigma v \rangle}{4} U (1 - zf)^2 - \frac{R(1-\eta)}{\eta}}$$

and the Lawson criterion as

$$n_\ell \tau = \frac{3kT \left[1 + (1 - fz) + f\right]\frac{(1-\eta)}{2\eta}}{\frac{\langle\sigma v\rangle}{4} U_t(1 - zf)^2 - \frac{R(1-\eta)}{\eta}}$$

and the Lawson criterion as

where U_t = total energy released = 22.4 MeV

and η = thermal conversion efficiency ≈ 0.3

The extent of power loss from the plasma due to these impurities can be estimated from the following equations:

For free-free bremsstrahlung, power-loss is given by

$$P_B = 4.86 \times 10^{-30} n_e T_e^{1/2} \frac{\sum_i z_i^2 n_i g_{ff}(z^2/T)}{\sum_i z_i n_i} \quad (W/cm^3)$$

where g_{ff} if the Gaunt factor to correct for quantum effects, and is a function of the ion temperature and impurity ion species. Values of g_{ff} are given by Karzaz and Latter.[10]

Recombination radiation generated between highly-stripped, high Z ions and plasma electrons,[11] and line radiation loss[12] from transitions of the type $\Delta n = 0$ in not fully ionized atoms, are given by

$$P_R \stackrel{\sim}{=} 1.3 \times 10^{-32} f \frac{z^4}{T_e^{1/2}} n_e^2 \quad (W/cm^3)$$

$$P_L \stackrel{\sim}{=} 2 \times 10^{-26} f n_e^2 \quad (W/cm^3)$$

respectively.

In addition to creating increased radiative cooling and increasing operating temperatures, gas atoms and high Z impurities can create a much more detrimental effect by accumulating on the

plasma periphery and inducing a beam-deposition instability.[13] Charge-exchange between cold background gases, mainly from the ion source of neutral beam injectors, together with the high Z impurities sputtered off vacuum walls, will create an effective impurity layer, limiting neutral beam deposition through the sequential process of local heating, charge exchange, more sputtering of wall material, and further impact ionization of the neutral beam. Work in this area by Post et al.[13] and Girard et al.[14] has been particularly illuminating. This impurity-driven instability, coupled with the inevitable 10% loss of neutral beam power through charge-exchange,[15] might severely limit neutral beam penetration. Many methods have been suggested to alleviate the problem of impurities,[16-18] but in the case of cold streaming deuterium gas from neutral beam injectors, differential pumping[19] using cryocondensation pumping at liquid helium temperatures is the only feasible method.

B. Cryocondensation Pumping for Neutral Beam Injectors

The recent success of neutral beam injection has placed great demand on improved vacuum systems and techniques, particularly in the form of cryocondensation pumping.[5]

The reasons for choosing cryopumping over other methods are many: Ion pumps give pumping speeds too small to be effective, and oil diffusion pumps are big and costly, with the furhter disadvantage of oil contamination from backstreaming.[6] Furthermore, failure of diffusion pump cold traps would almost certainly lead

to irreparable contamination of vacuum walls and delicate high voltage systems, whereas cryopumping failure only increases the partial pres sure of the pumped gases in the system.

The high energy, high current ion sources developed for the pro- duction of neutral beams[20] for fusion experiments require gas flows much in excess of the actual injected neutral ion flux. To remove this large gas load, typically tens of Torr-l/sec, will require pumping speeds for deuterium on the order of $\sim 3 \times 10^6$ liters/sec for the Tokamak Fusion Test Reactor (TFTR) 3-source beamline.[5]

Although large cryopumps have been built[20] and successfully op- erated, very little is known about the actual behavior of cryogenic deposits, particularly under CTR conditions.[5] Benvenuti and Calder[21], and Lee[22] have measured vapor pressures of H_2 at close to liquid-helium temperatures. They have found that the saturated vapor pressure roughly satisfies the Clausius-Clapeyron equation

$$\ln P_{sat} = -\frac{A}{T} + B \ln T + C \quad .$$

where A, B and C are constants.

Though further investigations on the effects of various heat loads and electron bombardment were made by Benvenuti and Calder,[23] and Erents and McCracken,[24] no cryopumping assembly has been operated in proximity of a large neutral-beam source, and in the presence of an additional intermittent temperature and possibly desorption effect[25] from large bursts of neutrons and gamma rays as is expected from TFTR.

C. Pumping Speed Requirements for TFTR 3-Source Beamline

Each beam line is divided into three chambers. A schematic can be found in Fig. 2. The three ion sources making up each beam line contributes a total of 90 Torr-liter/sec, neutralized deflected charge ions and vacuum wall desorption contributes an additional 9 Torr-liter/sec. The main requirement is set by the pressure in chamber 2-3.84 x 10^{-6} Torr.

The gas balance equations are[20]:

$$P_1(S_1 + C_{12}) - P_2 C_{12} = Q_1$$
$$- P_1 C_{12} + P_2 (S_2 + C_{12} + C_{23}) - P_3 C_{23} = Q_2$$
$$- P_2 C_{23} + (S_3 \pm C_{23}) P_3 = Q_3$$

Solving for a relative minimum total, subject to the constraint $S_1 = S_2$, we have

$$S_1 = 1.71 \times 10^6 \text{ liter/sec}$$
$$S_2 = S_3 = 7.93 \times 10^5 \text{ liter/sec}$$

We can see that these high pumping speeds are not attainable with diffusion pumps. A large large assembly of titanium sublimation pumps, pumping speeds of around 2 ℓ/cm^2-sec[26], is capable of giving such a high pumping speed, but the gettering assembly would be extremely unwieldy. Thus the only alternative is cryogenic pumps of total area 30 m^2, assuming a pumping speed of 6 T-l/sec-cm^2 which can be accommodated in the neutral-beam injector volume available.

II. KNOWN PROPERTIES OF HYDROGEN AND DEUTERIUM APPLICABLE TO
CRYOCONDENSATION PUMPING

The properties of normal* (n) H_2 and D_2 at around 4.2 K are of great interest in cryogenic engineering, especially in the area of cryocondensation pumping. Properties of nH_2 and nD_2 have been tabulated extensively.[27,28] In this chapter is a list of the triple points, saturated vapor pressures, and solid and liquid densities of nH_2 and nD_2.

A. Triple Point

Values recommended by the National Bureau of Standards[1] are listed below.

Species	Triple Point Temp., K	Triple Point Vapor Pressure (Torr)
nH_2	13.957	54.04
nD_2	18.71	128.5

The triple point of a one component system is defined when all three phases of the system are in equilibrium. From Gibbs phase rule

$$v = c - p + 2$$

*Hydrogen isotopes exist as a mixture of ortho and para configurations. This phenomenon is due to quantum mechanical exchange degeneracy and symmetry characteristics of the hydrogen molecular wave function.[29] The percentage of ortho-para concentrations in such a mixture is temperature dependent. Para-hydrogen and ortho-deuterium predominate at cryogenic temperatures.

where v = No. of degrees of freedom

                  c = No. of components

                  p = No. of phases

we have, since $c = 1$, $p = 3$

                  $v = 0$

which means that the one component system is invariant at this par-
ticular temperature.

B.   Vapor Pressure

The saturated vapor pressure, P_{sat}, can be quite accurately re-
presented by the equation

$$\ln P_{sat} = - \frac{A}{T} + B \ln T + c \qquad . \qquad (1)$$

down to liquid-helium temperatures.

Values of A, B, and C are

Species	Solid-vapor constants		
	$\underline{A}$	$\underline{B}$	$\underline{C}$ (Torr)
nH_2	98.63	1.982	5.832
nD_2	137.1	2.378	5.217

Equation 1 is defined by assuming a temperature-dependent latent heat
of sublimation, L, of the form[30]

$$L = R(A+BT)$$

where A and B are the constants listed above, and $R = 8.314$ J/mol-K.
Substituting into the Clausius-Clapeyron equation[31] yields

$$\frac{d\ln P_{sat}}{dt} = + \frac{A}{T^2} + \frac{B}{T}$$

$$\ln P_{sat} = -\frac{A}{T} + B\ln T + C$$

Vapor pressures below the triple point are often referred to as sublimation pressures.

C. Liquid and Solid Densities

Briggs et al have reviewed existing literature[1,32-34] and suggested the formulas

$$\rho_L = A_L - B_L T^2$$

and

$$\rho_s = A_s - B_s T^2$$

The constants are

Species	A_L	B_L	A_s	B_s
nH_2	0.0412×10^6	0.145	4.43×10^4	0.478
nD_2	0.0477×10^6	0.130	5.07×10^4	0.290

III. DESCRIPTION OF A TEST CRYOPUMP FOR TFTR

A. Cryopump Construction

Because of the diversity of conditions in the TFTR reactor en-
vironment under which future cryopumps will have to operate, a test
prototype has been designed and constructed by the LBL/LLL joint engi-
neering group. The objectives are to explore design and operations
problems and limitations, to test compatibility of the cryopump in
the proximity of a large neutral-beam source, and to investigate the
effect of large bursts of neutrons and gamma rays similar to that
expected from TFTR.

Figure 2 is a photograph of the cryopumping module. The primary
feature of this cryopump is the black copper chevron array, consisting
of 24 5" by 14" OFHC copper plates chemically blackened and bent 120°
vertically to provide a high-absorptivity thermal radiation shield.
This was designed so that gases, mainly deuterium from the neutral-beam
ion source, will transmit through the array while providing thermal
radiation isolation for the liquid-helium panel and cooling down the
incoming gas particles.

About 6" behind the chevron array is a double-wall quilted
stainless-steel panel through which circulates liquid-helium at 4.2 K.
This liquid-helium panel provides an effective cryopumping area of 2160
cm^2, to give a total pumping speed for deuterium of approximately 6.0
$1/cm^2$-sec.[5] Unlike other crypump designs,[35] this one does not provide
an inlet reservoir for the liquid helium. Instead, the liquid helium is

forced through the quilted envelope by its own vapor pressure, gene-
rated inside the supply dewar through normal boiloff. The reason
for this arrangement is simplicity. In future TFTR applications,
cryopumps will most probably have to be sub-cooled to below 4.2 K
to reduce hydrogen for liquid-helium internal storage. Instead,
liquid-helium is simply vapor pressure. The helium circuit will
be directly connected to a refrigerator through thermally isolated
transfer lines.[30] Such an arrangement is also important in conserving
helium.

Immediately behind the liquid-helium envelope, on the other
face of the box facing away from the chevrons, is another double-wall
stainless-steel panel through which circulates liquid-nitrogen. This
panel functions as a radiation shield for the liquid-helium panel.

To the sides of the liquid-helium panel are four liquid-nitrogen
cooled OFHC copper plates. These serve to complete the thermal
radiation assembly enclosing the liquid-helium panel. These copper
panels also make up the sides of the cryopump module and the 24
copper chevrons are also bolted to these plates.

Liquid-helium is supplied through a concentric dual bayonet
fitting attached to a flexible, vacuum-jacketed liquid-helium trans-
fer line manufactured by Cryolab Corp. The two-phase helium return
from the cryopump is allowed to exhaust to air through a 12 ft.
length of copper tubing in order to prevent upsetting the convection
loop in the helium circuit.[36] Liquid-nitrogen is supplied via an
Armaflex insulated teflon transfer line.

For temperature measurement, the liquid nitrogen surfaces are monitored with copper-constantan thermocouples, and the liquid-helium surfaces are provided with carbon resistors and silicon diodes supplied by Lake Shore Cryotronics. Their various locations are shown in Figure 9. An electrical current of 10 microamp. was used for the resistors and diodes. Self-heating was found to be negligible. In order to provide maximum thermal contact and to produce a uniform temperature environment the resistors and diodes were enclosed in copper hats soldered onto the liquid-helium surfaces. See Figure 8.

B. Measuring Systems

Static pumping-speed measurements were made with the cryopump installed in the neutral-beam test facility beam line (Figure 11) and with the cryopump module inside its own vacuum enclosure (Figure 5). Dynamic pumping speed measurements were made only with the cryopump installed in the neutral-beam line, the dynamic measurements were made with both the ion-source operating and idle.

Different gases, H_2, D_2 and N_2, were introduced through a leak valve, the exact amount of which was monitored by a thermal conductivity type flowmeter manufactured by the Hastings-Raydist Company (Model #H-50). This flowmeter was calibrated against a mercury bubble leak-rate apparatus (Figure 10) in the range 1 - 0.5 Torr-liter/sec. The flowmeter calibration thus obtained was found to be linear and almost independent of the gas species. Calibration data were obtained to within an accuracy of 10% (Appendix 2).

The pressure in the system was measured by an external glass-enclosed Bayard-Alpert-type ionization-gauge (Veeco) and a nude Bayard-Alpert-type ionization gauge (Varian). The Varian gauge was connected to a Lawrence Livermore Laboratory built fast ion gauge power supply with a risetime of less than 1 msec. The Veeco ionization guage was driven by a conventional power supply. A quadrupole mass analyser (Uthe Technology International) was also used to determine the residual gas components and to measure desorption species during a beam pulse. The locations of the ionization gauges and the mass analyser are shown in Figure 11.

A calibration for H_2, D_2 and N_2 for the two ionization gauges was made using a Barocel electronic manometer pressure gauge (Datametrics) which had been calibrated against an oil manometer in the pressure range 10^{-4} Torr. The Varian ionization gauge was calibrated using both its regular power supply and the LLL-build fast ionization gauge power supply. The results obtained were significantly different from the manufacturers recommended correction values. A list of the calibration results can be found in Table 7. A subsequent calibration using the same gauges on a different vacuum system yielded similar results, to within experimental uncertainties.

IV. TEST CRYOPUMP MEASUREMENTS

Static, dynamic and beam-desorption-effect measurements of the test cryopump were made. The pressure measuring equipment used were the calibrated ion gauges, the LLL-built fast-response ion-gauge supply, and a quadrupole mass spectrometer (Uthe Technology International), these various instruments were all described in the last section. The measurements were designed to find the pumping speed for H_2 and D_2, and to look for any desorption effects from a plasma beam passing approximately 36" from the condensed deuterium. Pressure measurements were made at room temperature, a correction for thermal transpiration, $(293/4.2)^{1/2}$, was not applied to the results since we were only interested in pumping speed measurements, not the absolute partial pressures at the surface of the condensate. The experiments were carried out both with the cryopump in its own vacuum assembly (static measurements only) and as part of the neutralizer cell of the neutral-beam injector Test Stand IIIA at the Lawrence Berkeley Laboratory (dynamic pumping speed and beam desorption measurements).

Before each chill-down with liquid-helium, a pressure of 1×10^{-4} Torr was obtained either with an LN_2-trapped diffusion pump (when cryopump is in its own vacuum assembly) or using the existing Test Stand IIIA vacuum. The panel was then cooled with LN_2 until the thermocouples indicate a temperature at or near 77 K, at which time LHe cooling commenced.

A. Static Pumping Data

These measurements were carried out both with the cryopump in its own vacuum assembly, and with the cryopump installed in the beamline. 99.95% pure H_2 and D_2 were used. Gas flow was monitored by a calibrated Hastings flowmeter. The method used was to measure the equilibrium pressure at various gas inputs, and then applying

$$Q = P \times S(P) \tag{1}$$

Where Q = gas load

   S = pumping speed

   P = measured pressure X gauge correction

With the cryopump operating, a continuous gas load (leak) was admitted into the system, metered accurately by the flowmeter for approximately 30 sec. The pressure was then noted. In this way, by varying the leak and measuring the different pressures, a plot of P vs. Q can be obtained. A best fit slope can be obtained from this plot in the region of interest. The pumping speed can then be obtained using Equation 1. (See Figures 12-15)

We can see from the figures that the pumping speed is almost pressure independent in the range 1×10^{-5} to 1×10^{-4} Torr for deuterium, and in the range 1×10^{-5} to 1×10^{-4} Torr for normal hydrogen. Values of the pumping speed were:

Species	Pumping Speed (1/sec)
nD_2	$1.43 \pm 0.15 \times 10^4$
nH_2	$1.60 \pm 0.17 \times 10^4$

These values correspond to a pumping speed/unit panel area of:

Species	Pumping Speed/Unit Area $(1/sec-cm^2)$
nH_2	7.41
nD_2	6.62

B. Dynamic Pumping Speed Measurements

These measurements were performed with the cryopump mounted adjacent to the neutralizer cell on Test Stand IIIA, and with the neutralizer section valved off from the main sphere. The volume is estimated to by 840l. A gas pulse of about 6 toor-1/sec and 700 msec. was introduced at the plasma source position. The pressure rise of each pulse was measured by the ion gauges. The Varian nude ion-gauge was connected to the LLL-built fast-response ion-gauge supply (risetime = 1 msec). The voltage output of this fast-response supply was connected to an oscilloscope and a waveform digitizer (Quantalatch). This waveform digitizer enables the pressure pluse to be recorded and read out later at various intervals. The voltage-time data can then be converted into a pressure-time history curve.

The pumping speed was obtained from the decay portion of the pumpdown curve.

$$P = P_o \, e^{-(\frac{S}{V})t} \quad .$$

A plot on semilog paper of the pressure vs. time gave a straight line whose scope is

$$\frac{s}{v} \; \log_{10} e$$

where s = pumping speed, and v = volume. (Figures 17-18) as can be seen from thse plots, the data are a good fit to a single exponential at $P < 1 \times 10^{-4}$ torr.

The dynamic pumping speeds obtained in this way were:

Species	Pumping Speed (ℓ/sec)
nH_2	$1.66 \pm 0.07 \times 10^4$
nD_2	$1.27 \pm 0.10 \times 10^4$

C. Beam Desorption Experiment

A quadrupole mass analyser was used to monitor the residual gas species concentration in the vacuum chamber at Test Stand IIIA. A hydrogen plasma beam was used for the test so as not to confuse desorbed deuterium with those from the plasma beam. The cryopanel was loaded with deuterium, approximately 12 Torr-liters, before the beam shots. The mass analyser output was connected to a storage oscilloscope so as to record the species concentration changes during a plasma beam pulse. A hydrogen plasma beam was then fired and recorded by the quadrupole mass spectrometer. Figure 19. We can see from the figure that mass=4 peak changes very little during the hydrogen beam pulse. We can conclude from this that beam desorption of adsorbed deuterium from a cryopanel is almost negligible. The fact that the mass=4 peak returned to its original amplitude almost immediately after the plasma pulse indicates insignificant desorption.

V. NEUTRON DESORPTION AND REACTOR FLUX DIAGNOSTICS

A. Introduction

The neutron flux generated by the $D(T,n)^4He$ and $D(D,n)^3He$ nuclear fusion reactions will react with shielding materials, vacuum containment devices, cryogenic magnet materials and pumps, and neutral-beam injectors. The neutron irradiations not only cause radioactive handling problems, as in the case of the first wall and the containment vessel, but it will also slowly alter the composition and the operating characteristics of certain materials, such as NbTi filaments in superconducting magnets,[37,38] and various components of the neutral beam source. These changes in composition may very well be the limiting factor on the duty cycle of these various crucial components, they may also be detrimental to reactor operation.

The neutral-beam ion-sources will be subject to a particularly intense neutron flux from the reactor plasma. The injection duct and the opening in the torus (Figure 23) for refueling would provide an aperture in the shielding of the plasma vacuum containment vessel through which neutrons and gamma radiation can escape. Most of this radiation streaming down the injection duct will emerge unattenuated, only a fraction will strike the walls of the duct and undergo scattering or various other reactions. The neutron spectrum for this process is shown in Figure 22.[39] This source of radiation, together with the fraction transmitted through shielding, has been estimated to be at 5×10^{11} neutrons/cm^2-sec and 1×10^{11} photons/cm^2-sec.[39] The flux of this streaming radiation at various locations can be found in Figure 24. In addition to neutrons and gammas generated

from the plasma, streaning neutrons are also produced by the $D(d,n)^3$He reactions taking place on the beam dump, and from $D(t,n)^4$He reactions between tritium atoms streaming down the injection duct and the incoming neutral deuterium beam. This additional source is expected to be quite small, on the order of 5×10^7 neutrons/cm^2 -sec.

The effects of this source of fast streaming neutrons from the torus are many:

1. The neutral-beam ion-source materials will be gradually be poisoned by activation products and altered through radiation damage. This can conceivably alter the operating characteristics of the ion-sources.

2. Neutron and gamma heating of liquid-helium in cryopumps, though insignificant compared with the steady thermal radiation load,[25] would increase liquid-helium consumption and cause a higher H_2 vapor pressure in the vacuum because of the temperature increase.

3. A more drastic effect on the cryopumps would be the desorption produced by knock-on neutrons.

Neutron damage and increased thermal loads on cryopumps are quite well understood. Activation poisoning and neutron helium heating can be mitigated by improved shielding, but the desorption effect on the cryocondensed deterium may limit the use of cryopumping to well-shielded areas away from the beam ducts, where their primary purpose is lost and their effectiveness decreased.

B. Berkeley Research Reactor Experiment

In order to ascertain the effect of fast neutrons and gamma radiation
on the absorbed deuterium gas molecules, an experiment has been planned
by the LBL CTR-staff to irradiate the deuterium-loaded cryopanel assembly
at the Berkeley Research Reactor. It is hoped that results obtained from
this experiment will provide data and information on how a cryopanel will
respond to an actual radiation load.

Neutron induced radiation damage on solids has been studied exten-
sively.[40,41] It is reasonable to expect that neutrons will also interact
with the amorphous condensed gases as they do with atoms in a solid. The
primary knock-on deuterium molecules produced from neutron-deuteron col-
lisions will migrate and break more adsorption bonds, creating what
is comparable to a collision cascade in radiation damage. This may
lead to release from the condensation surface, lowering pumping speeds
and raising the vapor pressure of the various gases, particular deuterium,
in the vacuum. This effect, if allowed to happen on a large scale,
would seriously undermine the effectiveness and appeal of cryocondensation
pumping--mainly its high pumping speed. If experiments were to prove
that neutron knock-on collisions do give large desorption effects, current
TFTR reactor designs, especially those for the neutral-beam injection
systems,[19] will have to be revised to include more shielding and
to locate the cryopumps in areas with the lowest neutron flux.

The Berkeley Research Reactor (BRR) (Figure 20) produces an intense
pulse of neutrons and gamma rays in a Gaussian pulse with a half width
of about 12.6 msec. Pulses are generated by pneumatically ejecting a
control rod from the reactor core and placing it in a prompt-critical

condition, up to $3.00 above delayed critical. The resultant power excursion is terminated due to the large negative temperature coefficient of reactivity of the uranium-zirconium fuel-moderator assembly. The result of this power excursion is a 12.6 msec-halfwidth neutron and gamma pulse with an integral power of approximately 16.3 MW-sec. Data[42] from previously measured reactor pulses are given in Figure 21, as measured in the Exposure Room. Figure 22 is a plot of the spectrum of a BRR neutron pulse, assuming negligible degradation by the moderator. Also in the Figure are the expected TFTR streaming and transmitted neutron spectrum. Although the BRR fast neutron pulse has a fast neutron fluence of 0.72×10^{11} neutrons/cm^2-pulse, which is comparable to what is expected from TFTR-1.16×10^{11} neutrons/cm^2-pulse, the BRR spectrum is much richer in thermal neutrons which could be eliminated by borated polyethylene blocks and lead sheets in the actual experiment. The measured gamma dose of the BRR at 2 feet from the core in the Exposure Room region corresponds to a gamma flux of 1.74×10^{13} photons/ cm^2 -pulse, assuming a gamma spectrum corresponding to that from prompt fission. It can also be seen that the reactor fast neutron spectrum is much softer (has more lower-energy particles) than the one expected from TFTR.

C. Reactor Pulse Measurements

Accurate measurements of the neutron spectrum and the gamma flux of a $3 pulse were made in order to ascertain the neutron spectrum in which the cryopump will be exposed. Measurements were only made in the Exposure Room Facility of the Berkeley Research

Reactor. The method used was the activation of cadmium covered ^{197}Au and ^{115}In foils, and bare ^{197}Au foils

from a threshold-detection packet foil (Reactor Experiments, Inc.), plus ^{27}Al foils. ^{7}LiF thermoluminescent dosimeters (TLD's) were used to measure the total gamma flux. Table 25 contains a list of the foil materials, activation reactions, products, cross-sections used for calculations, and threshold energies. The cross-section values were taken from Calamand.[43]

The threshold foils were carefully weighed and enclosed in a plastic vial approximately 1" in diameter which was then placed 24" from the reactor core indentation in the Exposure Room Facility and subjected to a \$3 pulse. The foils were then retrieved and the photopeaks counted in a calibrated NaI(Tl) single-channel scintillation counter (Figure 26). This assembly uses two NaI(Tl) crystals placed facing each other in order to improve the counting efficiency. The product nuclides counted were as follows:

Sample	Reaction	Product	t1/2	Peak (MeV) Counted	E_{eff}(MeV)
^{27}Al	(n,p)	^{27}Mg	9.5	1.013	3.3
^{27}Al	(n,α)	^{24}Na	15hr	1.37	8.7
^{115}In(Cd)	(n,n')	^{115m}In	4.5hr	0.335	1.0

Gamma rays produced scintillations were amplified successively by the photomultiplier and the linear amplifiers. The amplified signals were then fed into the single channel analyser and an oscilloscope where the gamma energy spectrum was displayed. The single channel analyser window was then narrowed on to the gamma peak

we were interested in so that only counts due to that particular peak will be registered. Both NaI(Tl) scintillation counters were set this way. Counts were then taken with two timer controlled scalars.

A correction factor,

$$e^{+\lambda t}$$

was used to correct for decay between activation product nuclide production and the time of counting.

An abundance ratio ,

$$\frac{1}{\gamma\text{-ray abundance}}$$

was also used to correct for less than 100% gamma ray abundance in the decay spectrum.

A final correction factor, C_{sc}, was used to correct for counter efficiency. Since not all the gammas produced by the radionuclides are counted by the scintillation counter, a calibration curve was made using various calibrated sources to produce a γpm/cpm(Csc) vs gamma ray energy curve.

Hence, for the NaI(Tl) sintillation counted nuclides, the activity at the time of the pulse, in disintegrations per minute, is given by

$$A_0 = (cpm) \times e^{+\lambda t} \times \frac{1}{\gamma\text{-ray abundance}} \times C_{sc}$$

where cpm=number of counts per minute at the time of counting

The ^{197}Au and cadmium-covered ^{197}Au foils were also counted in a coincidence spectrometer (Figure 27), and the results compared well with those from the scintillation detectors. The product nuclides

counted were:

Sample	Reaction	Product	t1/2	(MeV) β-γ energy	γ-energy abundance	(b)
^{197}Au	cn,γ)	^{198}Au	2.7d	0.412, no β energy discrimination	95%	86.88
^{197}AutCd	cn,γ)	^{198}Au	2.7d	same as above	95%	86.88

In the coincidence method, counts were taken with the and channels in coincidence with each other, both background and foils were counted this way. Then leaving the foil in place, counts were taken with the β and γ channels out-of-coincidence in order to measure the accidental coincidence effect. The source strength at the time of counting can then be found by

$$cpm = \frac{(\beta)(\gamma)}{(_{\beta\gamma})} \quad (cpm)$$

where (β) = number of beta particles with analysers in coincidence

(background corrected)

(γ) = number of gammas with analysers in coincidence

(background corrected)

$(_{\beta\gamma})$ = number of coincident counts with channels in

coicidence − number of coincidence (background corrected)

The abundance correction is 1/0.95. The decay correction was taken to be $e^{\lambda t}$, where t is the elapsed time between the reactor pulse and the time of counting.

The activity of the gold foils then is given by

$$A_o = (\text{cpm}) \times \frac{1}{0.95} \times e^{+\lambda 198_{Au}t}$$

The activity difference between the Cd-covered and the bare Au foils represents the contribution of the thermal flux, corresponding to the 86.88b cross section.

To calculate the fluence of the reactor pulse, we assume the pulse to be a delta function, producing $\eta \sigma \phi$ product nuclides instantaneously at the time of irradiation. We have

$$\frac{dN}{dt} = \eta \sigma \phi - \lambda N$$

$$N = \frac{\eta\sigma\phi}{\lambda}(1 - e^{-t_1}) = \eta\sigma\phi t_1$$

where t_1 = reactor pulse duration.

From $N = \eta\sigma\phi t_1$

we have $\qquad A_0 = \lambda N = \eta\lambda\sigma\phi t_1$

$$\phi t_1 = \frac{A_0}{\eta\sigma\lambda} = \frac{A_0 \, t_{1/2}}{\eta\sigma(0.693)}$$

where $\qquad \phi t_1$ = fluence of the \$3 reactor pulse

$\qquad A_0$ = dpm of product nuclide at time of pulse

$\qquad \sigma$ = cross section of the particular activation

$\qquad\qquad$ reaction

$\qquad \eta$ = the number of atoms in the foil

with ϵ = atomic abundance of isotope being irradiated

    A = Avogardro's number (atoms/mole)

    W = atomic weight

    m = mass of foil in grams

The TLD's were read on a Harshaw TLD readout unit. A calibration using similar ^{7}LiF TLD's was made at the ^{60}Co irradiation facility at the Lawrence Berkeley Laboratory in our range of interest. Figure 28 is a graph of this calibration. Gamma dose readouts from the reactor pulse were read directly from this calibration curve.

Using this method, the neutron spectrum and the integrated gamma dose of a \$3 reactor pulse was measured. The results are shown in Figure 29.

The > 8.7 MeV fluence shows a large deviation from what is expected, that is, < 1.1×10^{12} neutrons/cm^2, because of the lack of correction for the continuous Compton peak of the 2.75 MeV gamma peak of ^{24}Na.

The counting error was estimated using

$$\Delta S = \frac{S+2B}{S} (100) \quad (\%)$$

S = counting rate (background corrected)

B = background counts

Conclusion

A cryocondensation pumping design has been proved to be practical both in operation and in meeting pumping speed requirements called for in fusion reactor experiments. Various instrumentation for this application have been evaluated and tested for measurements and diagnostics. Beam interaction with the absorbed deuterium has been found to be minimal. A method has also been developed whereby the neutron spectrum and gamma dose which will be used for a future knock-on desorption experiment can be evaluated.

APPENDIX I

0.5 W Allen-Bradley resistors were used for monitoring
low temperatures. These were calibrated by immersion in
LN_2, LHe, room temperature and an ice bath. The resulting
data were fitted to an empirical formula given be Clemment[44]

$$\ln R + \frac{K}{\ln R} = A + B/T \quad .$$

A computer program was written to fit the above constants
to the experimental data. A list of the resistance vs.
temperature was obtained.

The silicon diodes were calibrated by the manufacturer.
A plot of one of the calibrations is included.

APPENDIX II

The Hastings flowmeter was calibrated against a mercury leak apparatus as shown in Figure 10. The time needed for the mercury bubble to traverse the 1 cm^3 volume tube was recorded by a stop clock. The pressure difference between the beginning and the end of the run and the reading on the Hastings flowmeter were noted. The results of this calibration for D_2 and H_2 are included in Figures 32 and 33.
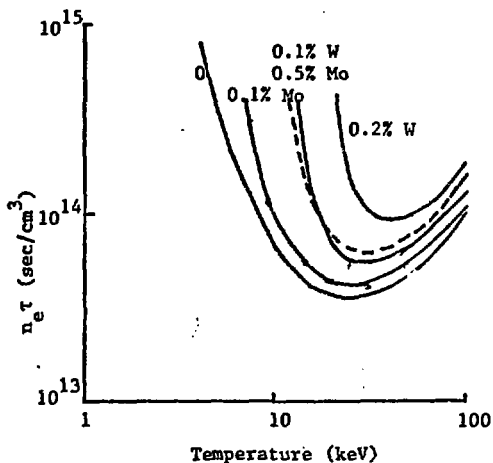
Lawson condition for a D-T reactor with various
high Z impurities
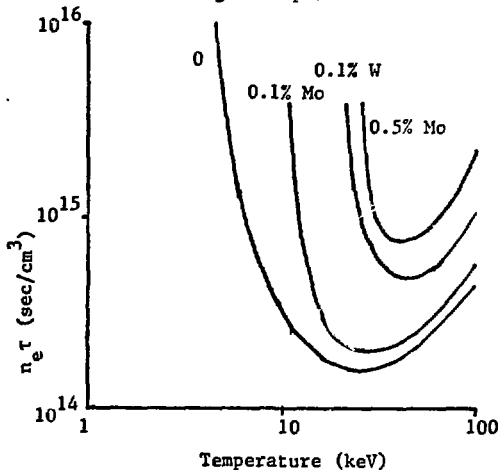
Ignition condition for a D-T reactor with various
high Z impurities

Fig.1   EFFECT OF HIGH Z IMPURITIES ON THE IGNITION
AND LAWSON CONDITIONS
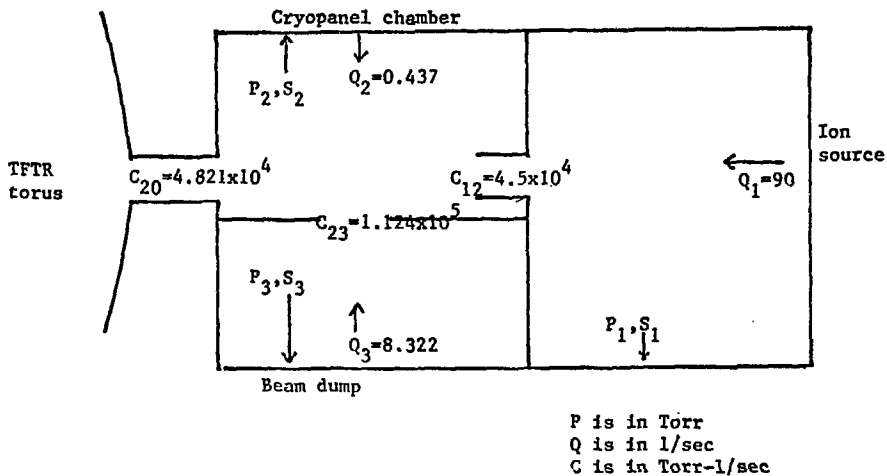
Fig. 2   SCHEMATIC OF NEUTRAL BEAM INJECTION UNIT SHOWING
VARIOUS GAS LOADS AND CONDUCTANCES
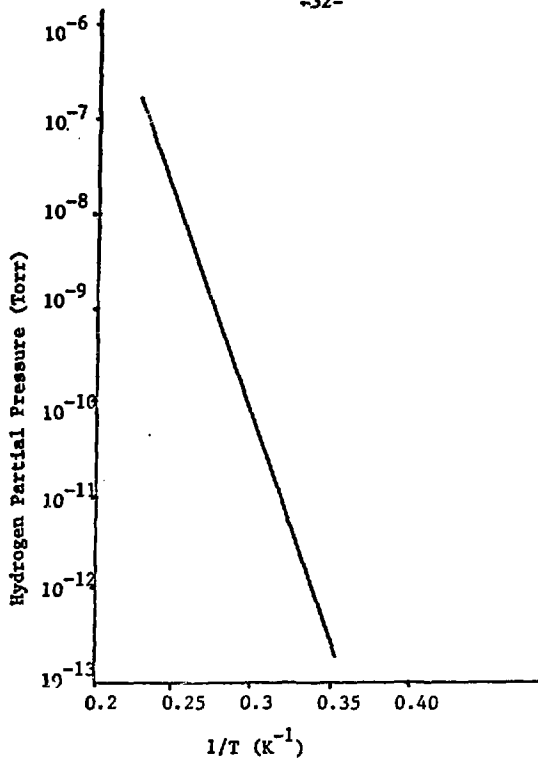
Fig. 3   SATURATED VAPOR PRESSURE VS. TEMPERATURE FOR

HYDROGEN
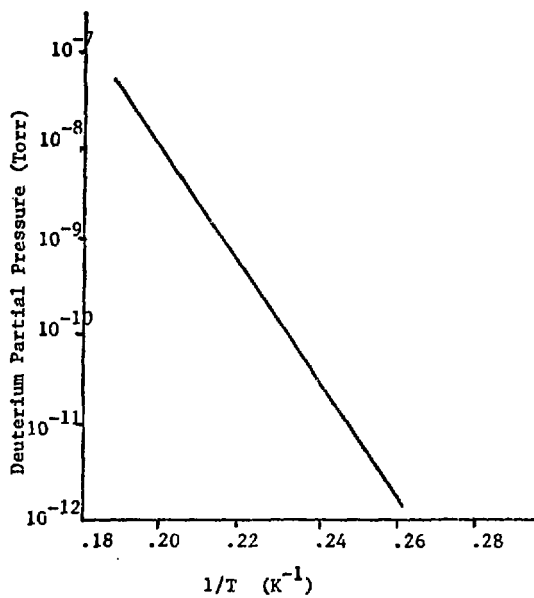
Fig. 4   SATURATED VAPOR PRESSURE VS. TEMPERATURE FOR

DEUTERIUM
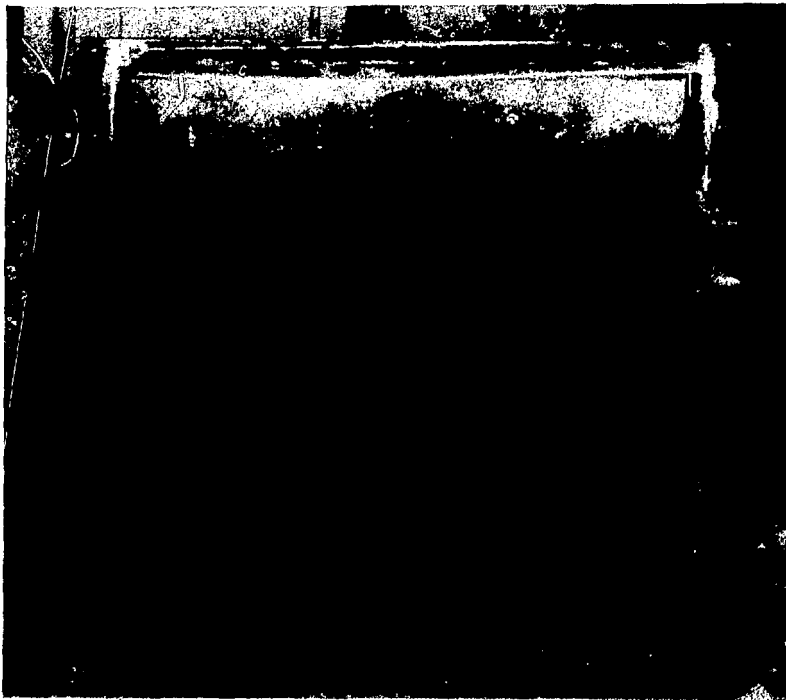
CBB 774-3650

Fig. 5
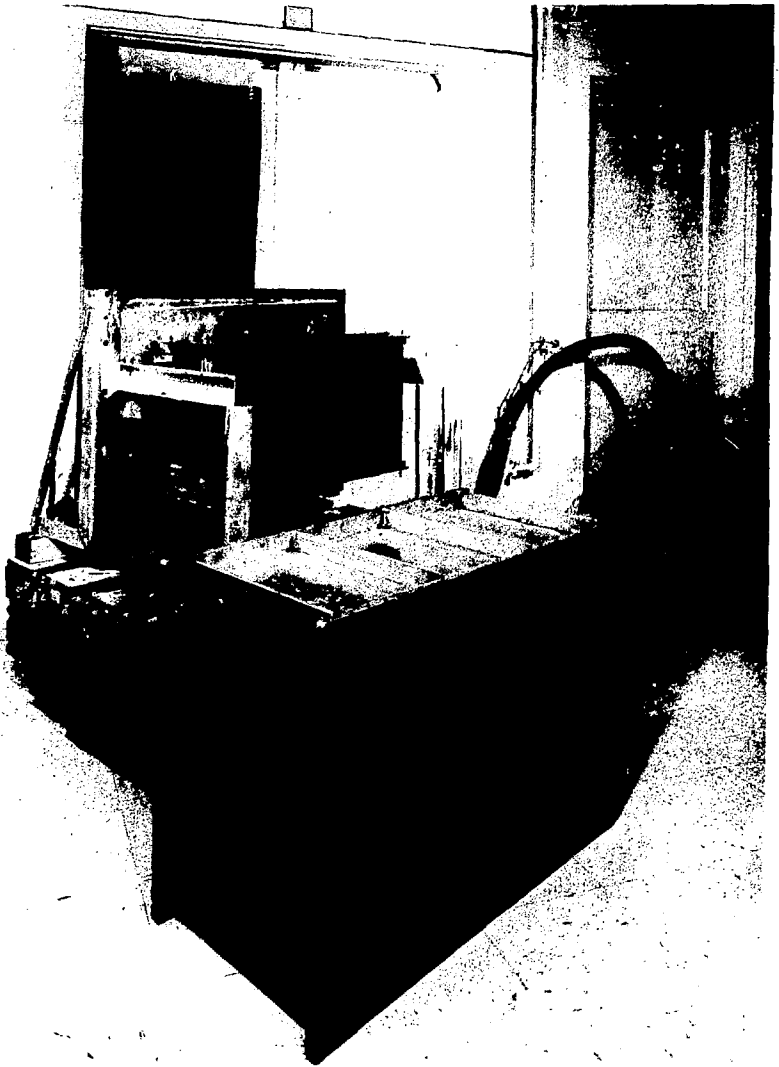
CBB 774-3652

Fig. 6

Gas Species	Outside B-A Gauge	Nude B-A Gauge
D_2	3.56±0.07	4.01±0.24
H_2	3.36±0.27	3.74±0.11
N_2	1.54±0.06	1.70±0.03

BAYARD-ALPERT IONIZATION GAUGE CALIBRATION FACTORS

Fig. 7
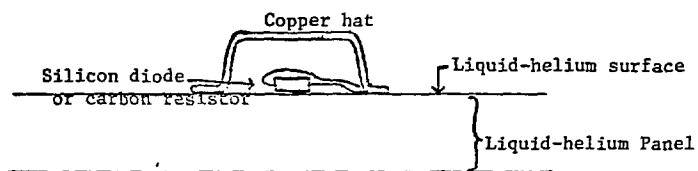
COPPER-HAT ENCLOSURE FOR SILICON DIODE OR CARBON RESISTOR

Fig. 8
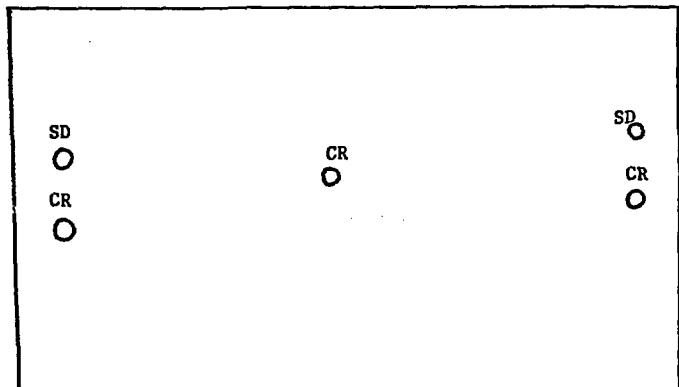
Back of stainless steel LHe panel
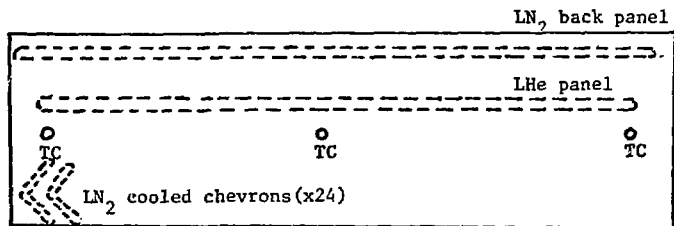
Top of cryopump assembly

SD = silicon diode
CR = carbon resistor
TC = thermocouple

LOCATION OF VARIOUS TEMPERATURE DIAGNOSTICS

Fig. 9
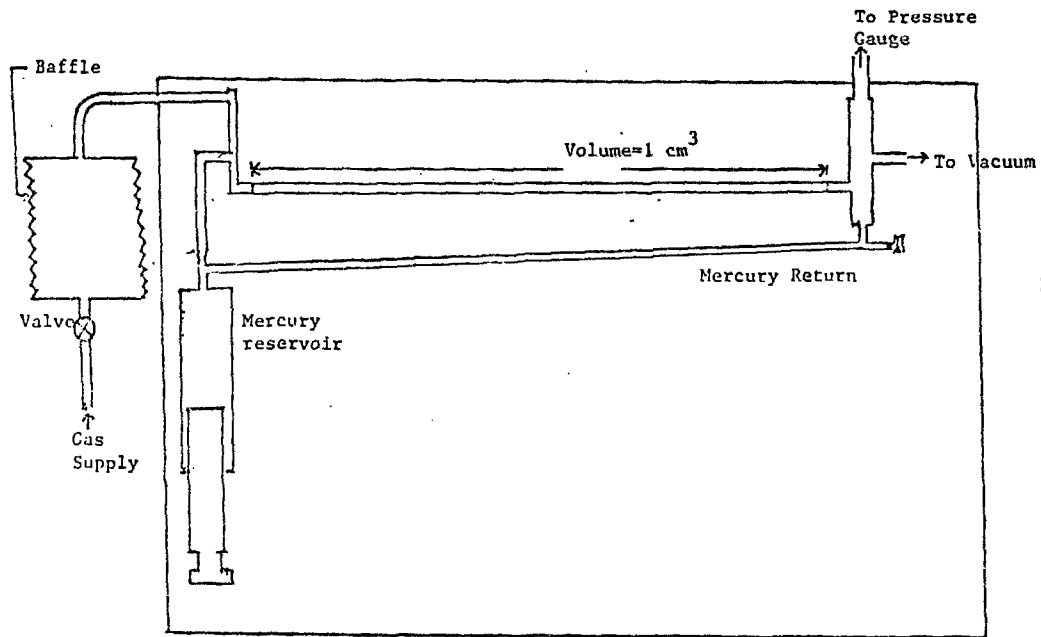
Fig. 10   MERCURY BUBBLE LEAK FLOWMETER
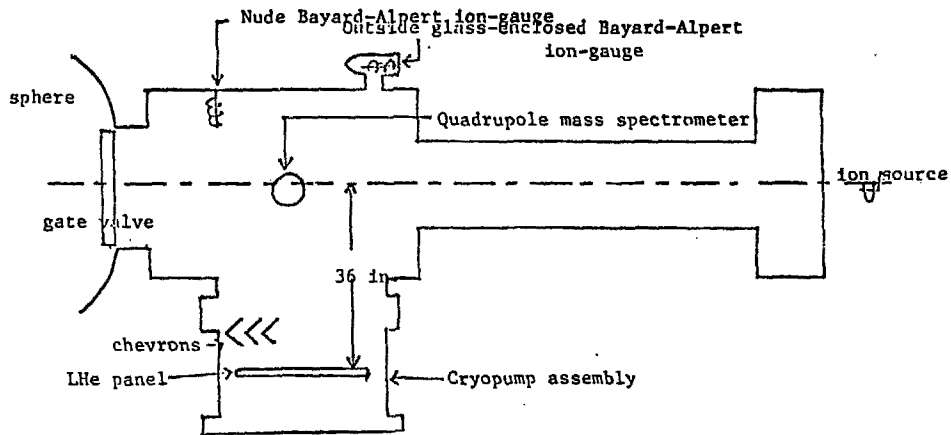
(Top view)

LOCATION OF CRYOPUMPING ASSEMBLY IN NEUTRAL BEAM
TEST FACILITY IIIA BEAMLINE

Fig. 11
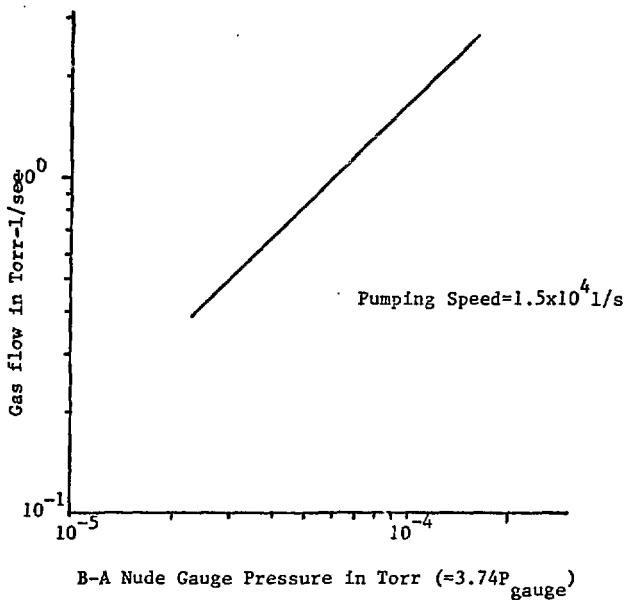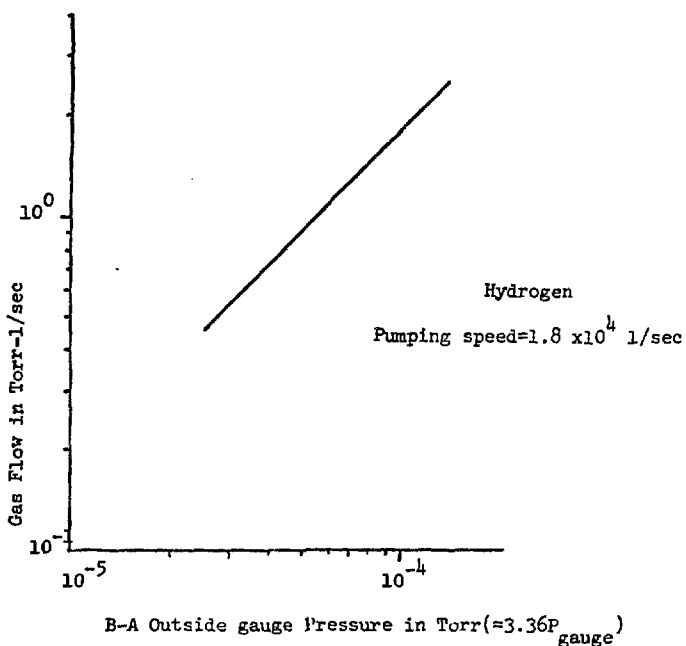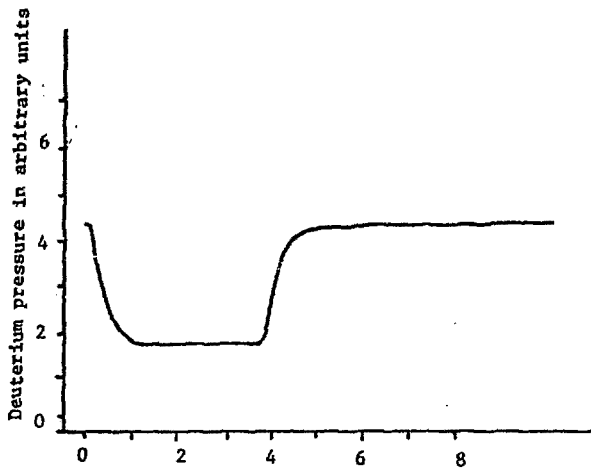
PUMPING SPEED FOR HYDROGEN

Fig. 12

Pumping Speed=1.3×10^4 l/s

B-A Nude Gauge Pressure in Torr (=4.01P$_{gauge}$)
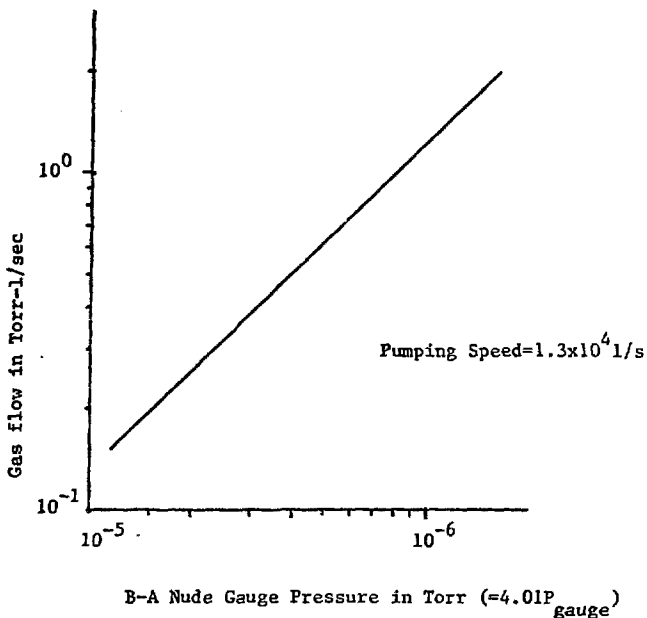
PUMPING SPEED FOR DEUTERIUM

Fig. 13
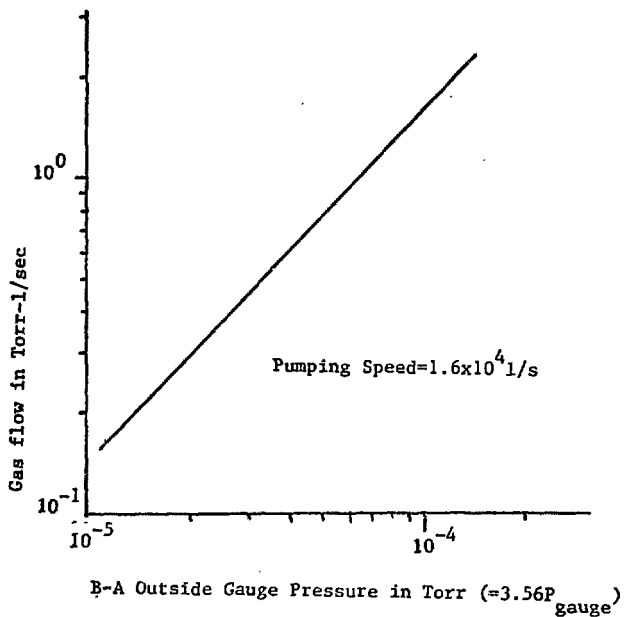
PUMPING SPEED FOR DEUTERIUM

Fig. 14

PUMPING SPEED FOR HYDROGEN

Fig. 15

Time (0.2 sec/division)

DEUTERIUM ION-SOURCE PULSE, BEAMLINE OPEN TO SPHERE
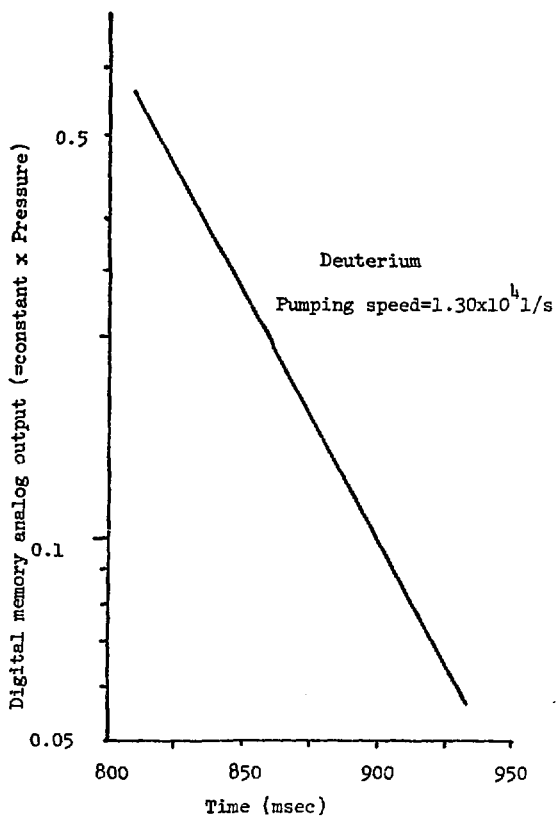

Time (0.2 sec/division)
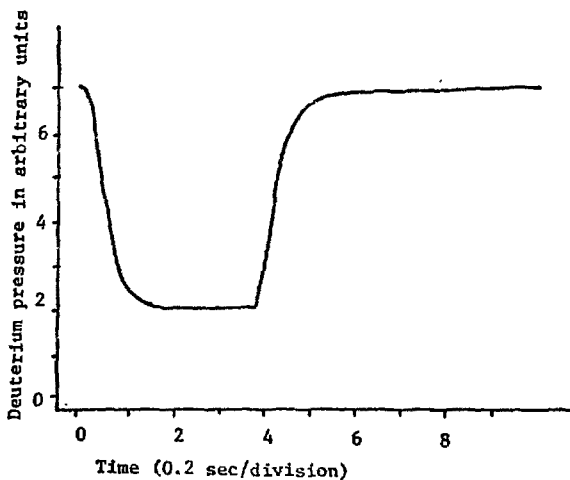
DEUTERIUM ION-SOURCE PULSE, BEAMLINE CLOSED TO SPHERE

PRESSURE HISTORY CURVES USED FOR MEASUREING DYNAMIC
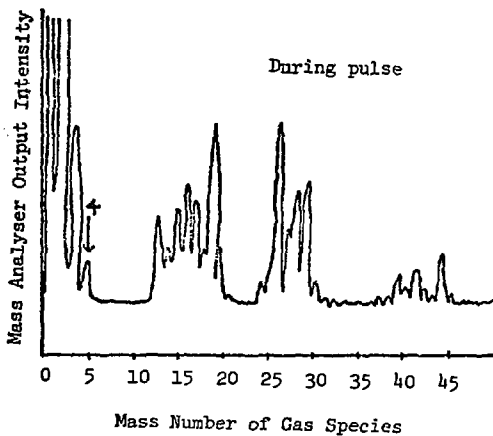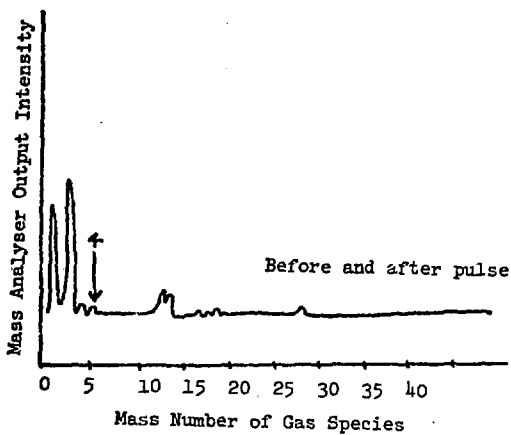PUMPING SPEEDS
Fig. 16
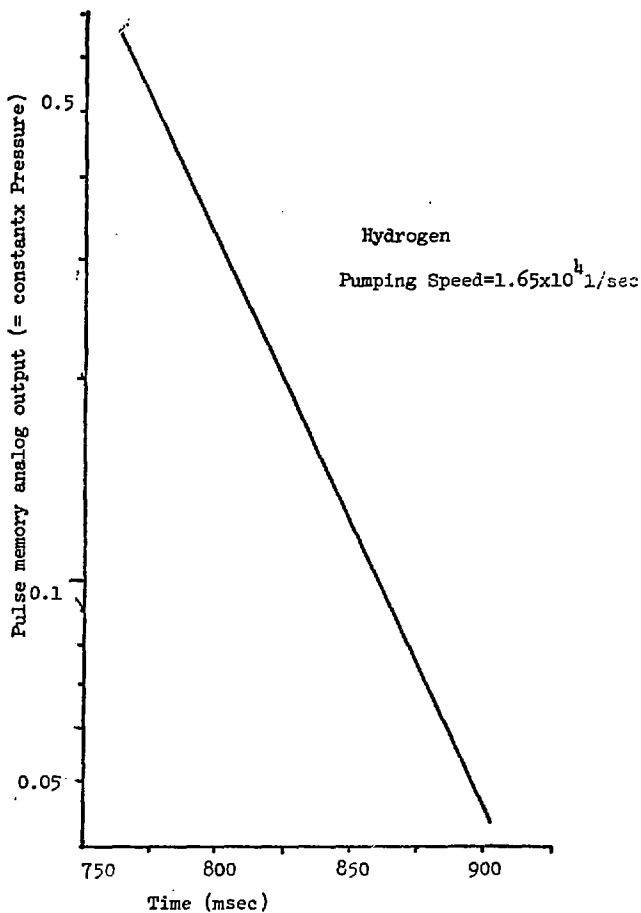
DYNAMIC PUMPING SPEED MEASUREMENT FOR HYDROGEN

Fig. 17

DYNAMIC PUMPING SPEED MEASUREMENT FOR DEUTERIUM

Fig. 18

Mass Analyser Output of a Hydrogen-gas operated
Ion-source and Deuterium-gas Loaded Cryopanel

Fig. 19
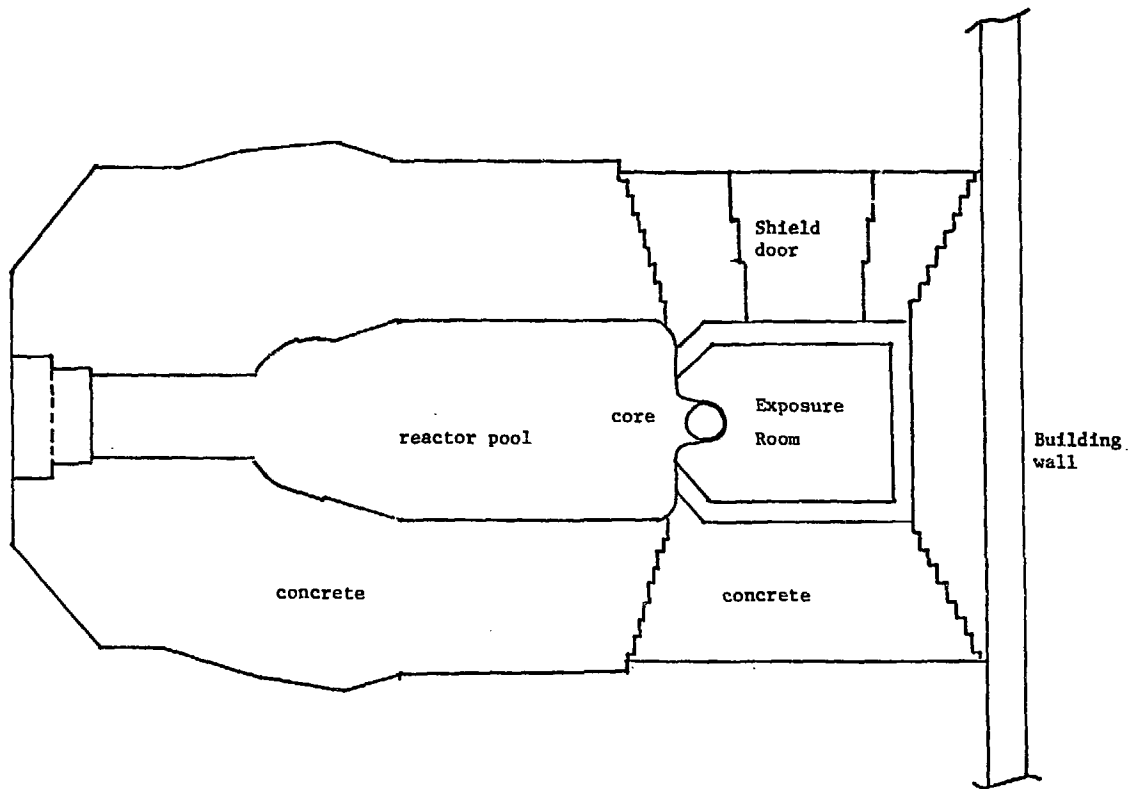
Fig. 20   TOP VIEW OF THE BERKELEY RESEARCH REACTOR

Distance From Core in.	Thermal Neutron Fluence n/cm^2	3.0 MeV Neutron Fluence n/cm^2
24	7.67×10^{11}	13.8×10^{11}
36	4.37×10^{11}	5.86×10^{11}
48	2.69×10^{11}	3.15×10^{11}

BERKELEY RESESRCH REACTOR INTEGRATED NEUTRON

FLUENCE

Fig. 21
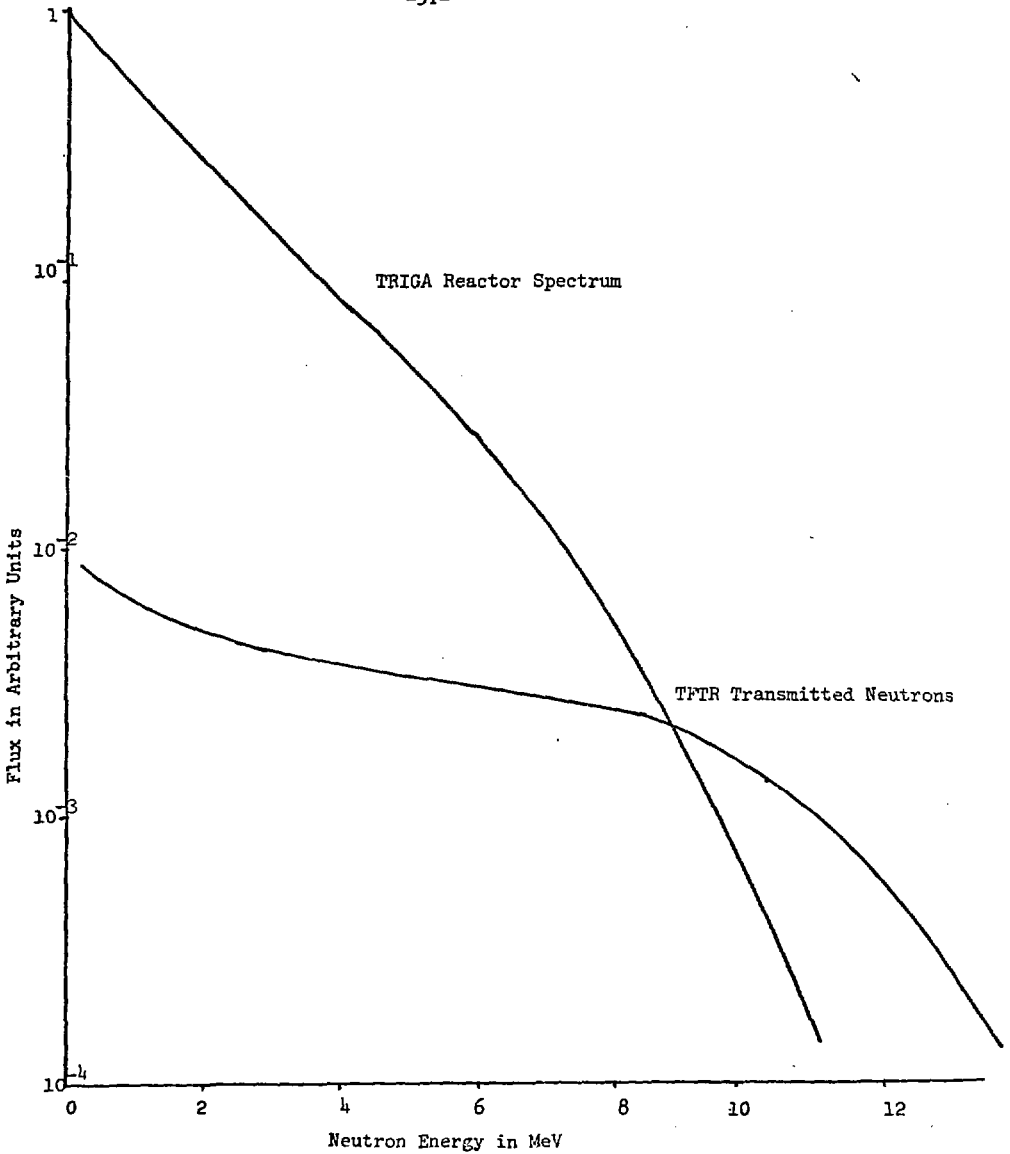
COMPARISON BETWEEN TFTR AND TRIGA NEUTRON SPECTRUM

Fig. 22

Diagram showing the existence of a neutral beam injection aperture
allowing unshielded, unattenuated neutrons to escape

Fig. 23

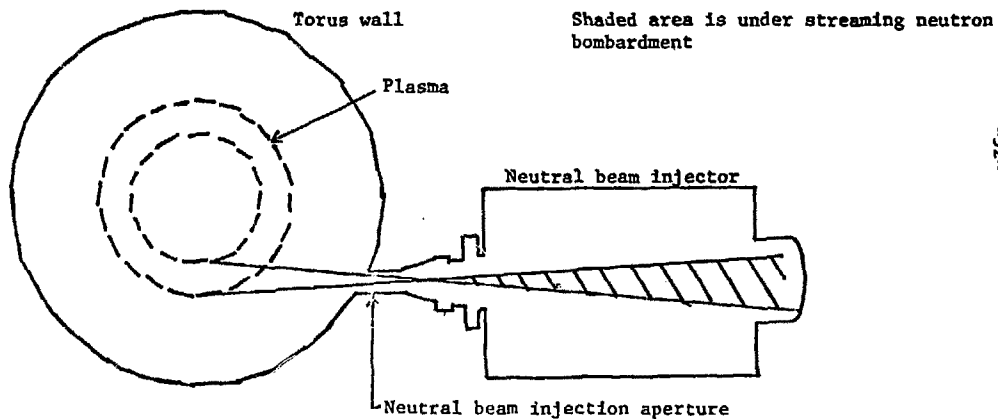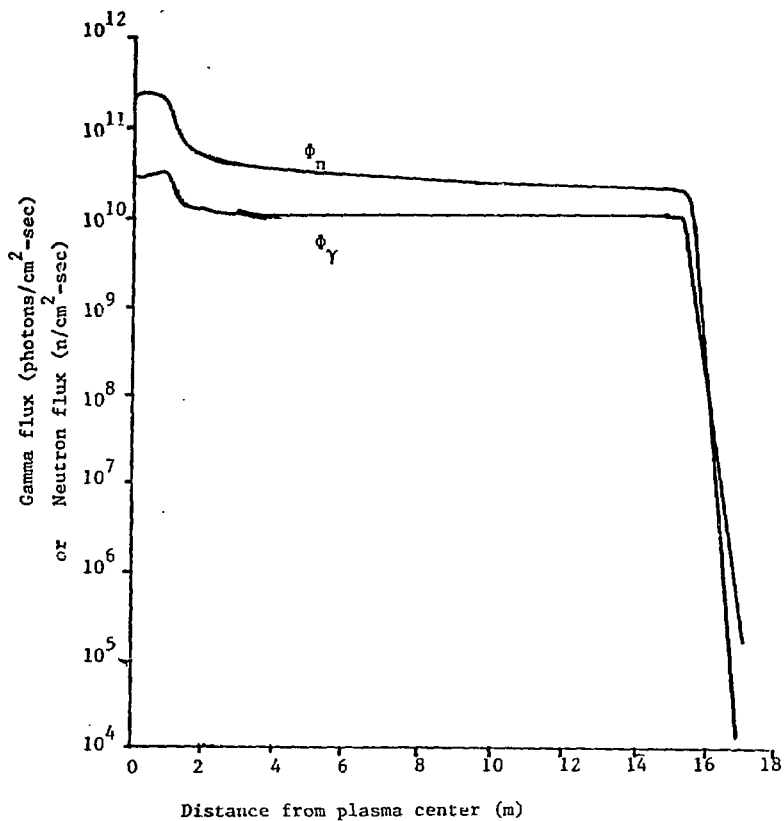TOTAL NEUTRON AND GAMMA FLUX AROUND TFTR (NO SHIELDING)

Fig. 24

Sample	Reaction	Product	$t_{1/2}$	Peak counted	E_{eff}(MeV)	σ
^{27}Al	(n,p)	^{27}Mg	9.5 min	1.013(30%)	3.3	3.1 mb.
^{27}Al	(n,α)	^{24}Na	15 hr.	1.37(100%)	8.7	0.48 mb
^{115}In(Cd)	(n,n')	^{115m}In	4.5 hr.	0.335(50%)	1.0	171 mb
^{197}Au	(n,γ)	^{198}Au	2.7 Day	0.412(95%)+β	0.25 eV	87 b
^{197}Au	(n,γ)	^{198}Au	2.7 day	0.412(95%)+β	0.25<E<0.4 eV	87 b

Fig. 25   LIST OF FOIL MATERIALS USED FOR NEUTRON SPECTRUM MEASUREMENT
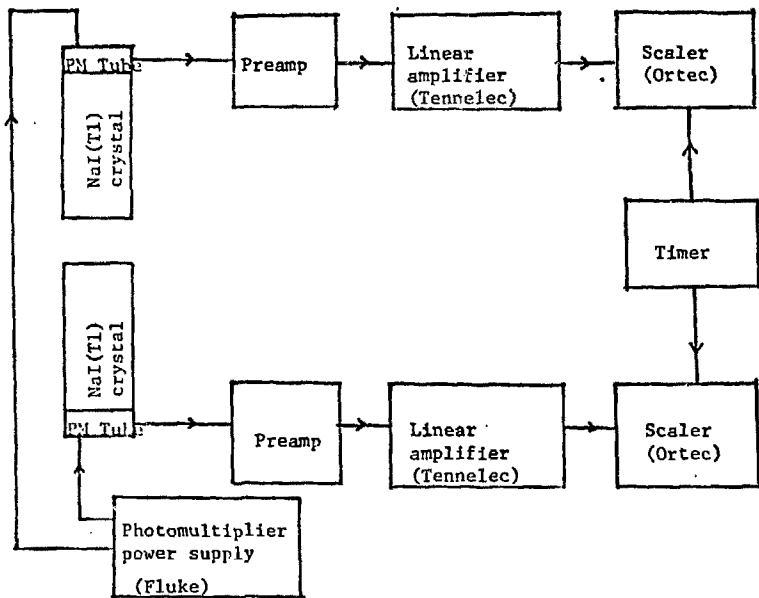
SCHEMATIC OF NaI(Tl) SCINTILLATION COUNTER

Fig. 26
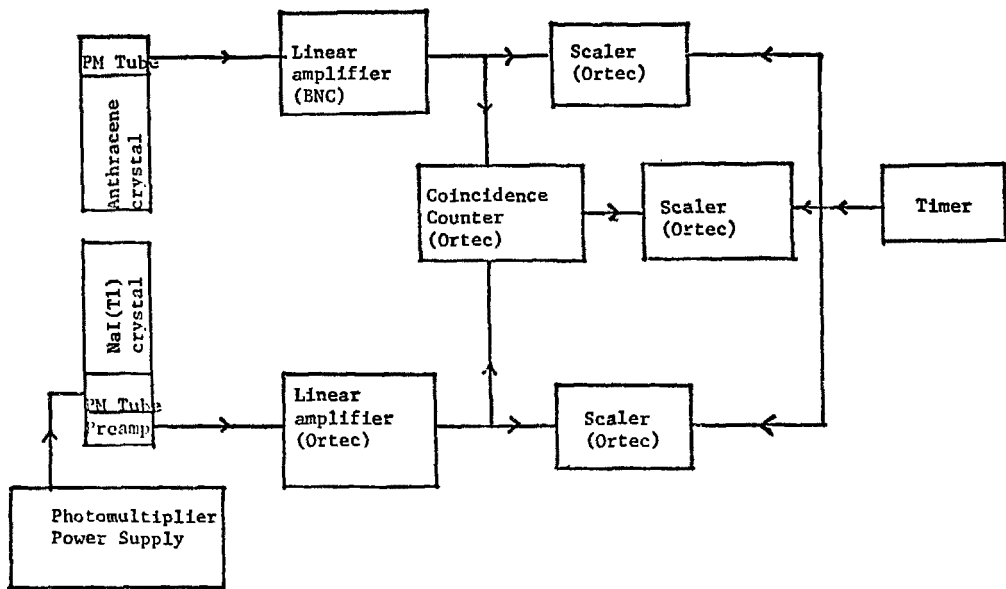
SCHEMATIC OF β-γ COINCIDENCE COUNTER

Fig. 27

Background corrected TLD reading in μC
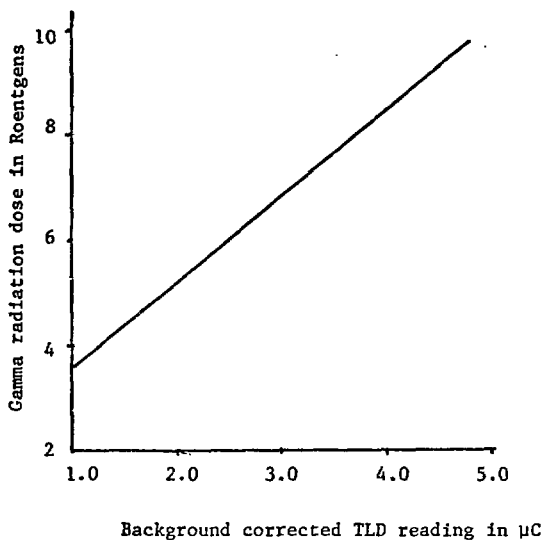
CALIBRATION FOR THERMOLUMINESCENT DOSIMETER
LIGHT OUTPUT vs. DOSE

Fig. 28

Foil	Energy Range	Neutron flux $(n/cm^2$-pulse)
$^{115}In(Cd)$	> 1 MeV	1.91×10^{12}
^{27}Al	> 3.3 MeV	1.14×10^{12}
^{24}Na	> 8.7 Mev	5.80×10^{12}
^{198}Au	thermal	1.10×10^{11}

Method	Energy Range	Gamma Flux $(photons/cm^2$-pulse)
TLD	Entire spectrum	2.16×10^{13}

RESULTS OF A REACTOR PULSE MEASUREMENT USING
THE FOIL ACTIVATION METHOD

Fig. 29
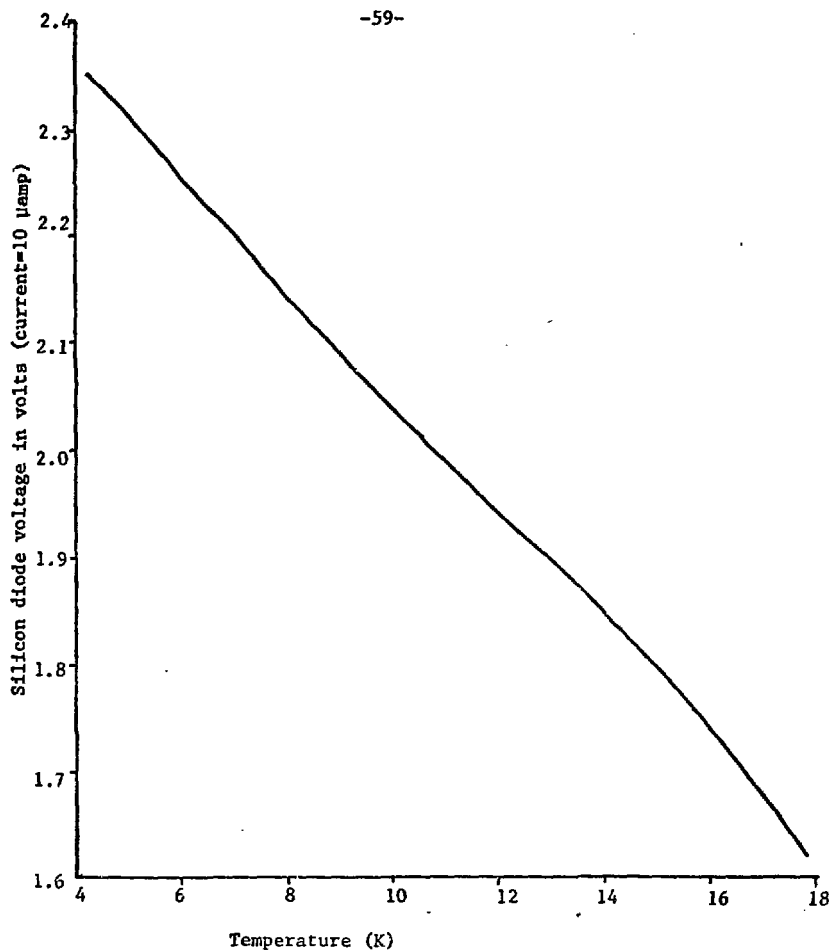
SILICON DIODE TEMPERATURE-VOLTAGE CURVE

Fig. 30

EMP. CALIBR. BASED CN .3250E+03 OHMS AT .293E+03 AND
.4160E+03 CHMS AT .770E+02 AND .5722E+04 OHMS AT .420E+01

| R IN OHMS	T IN KELVIN	R IN OHMS	T IN KELVIN	R IN OHMS	T IN KELVIN	h
5600	.4244E+01	5640	.4229E+01	5680	.4215E+01	
5601	.4244E+01	5641	.4229E+01	5681	.4215E+01	
5602	.4243E+01	5642	.4229E+01	5682	.4214E+01	
5603	.4243E+01	5643	.4228E+01	5683	.4214E+01	
5604	.4243E+01	5644	.4228E+01	5684	.4214E+01	
5605	.4242E+01	5645	.4228E+01	5685	.4213E+01	
5606	.4242E+01	5646	.4227E+01	5686	.4213E+01	
5607	.4241E+01	5647	.4227E+01	5687	.4212E+01	
5608	.4241E+01	5648	.4226E+01	5688	.4212E+01	
5609	.4241E+01	5649	.4226E+01	5689	.4212E+01	
5610	.4240E+01	5650	.4226E+01	5690	.4211E+01	
5611	.4240E+01	5651	.4225E+01	5691	.4211E+01	
5612	.4240E+01	5652	.4225E+01	5692	.4211E+01	
5613	.4239E+01	5653	.4225E+01	5693	.4210E+01	
5614	.4239E+01	5654	.4224E+01	5694	.4210E+01	
5615	.4238E+01	5655	.4224E+01	5695	.4210E+01	
5616	.4238E+01	5656	.4224E+01	5696	.4209E+01	
5617	.4238E+01	5657	.4223E+01	5697	.4209E+01	
5618	.4237E+01	5658	.4223E+01	5698	.4209E+01	
5619	.4237E+01	5659	.4222E+01	5699	.4208E+01	
5620	.4237E+01	5660	.4222E+01	5700	.4208E+01	
5621	.4236E+01	5661	.4222E+01	5701	.4207E+01	
5622	.4236E+01	5662	.4221E+01	5702	.4207E+01	
5623	.4236E+01	5663	.4221E+01	5703	.4207E+01	
5624	.4235E+01	5664	.4221E+01	5704	.4206E+01	
5625	.4235E+01	5665	.4220E+01	5705	.4206E+01	
5626	.4234E+01	5666	.4220E+01	5706	.4206E+01	
5627	.4234E+01	5667	.4220E+01	5707	.4205E+01	
5628	.4234E+01	5668	.4219E+01	5708	.4205E+01	
5629	.4233E+01	5669	.4219E+01	5709	.4205E+01	
5630	.4233E+01	5670	.4219E+01	5710	.4204E+01	
5631	.4233E+01	5671	.4218E+01	5711	.4204E+01	
5632	.4232E+01	5672	.4218E+01	5712	.4204E+01	
5633	.4232E+01	5673	.4217E+01	5713	.4203E+01	
5634	.4232E+01	5674	.4217E+01	5714	.4203E+01	
5635	.4231E+01	5675	.4217E+01	5715	.4202E+01	
5636	.4231E+01	5676	.4216E+01	5716	.4202E+01	
5637	.4230E+01	5677	.4216E+01	5717	.4202E+01	
5638	.4230E+01	5678	.4216E+01	5718	.4201E+01	
5639	.4230E+01	5679	.4215E+01	5719	.4201E+01	

Fig. 31
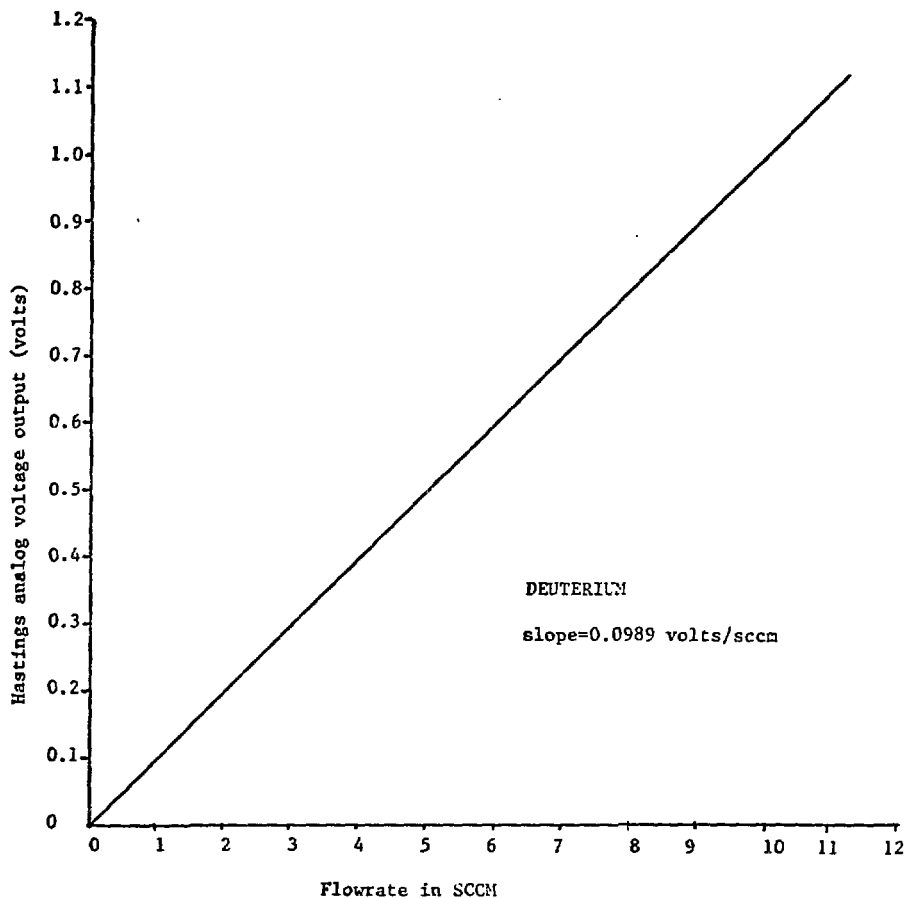
Fig. 32 HASTINGS FLOWMETER CALIBRATION (ANALOG OUTPUT vs FLOWRATE AS MEASURED BY THE MERCURY BUBBLE LEAK)
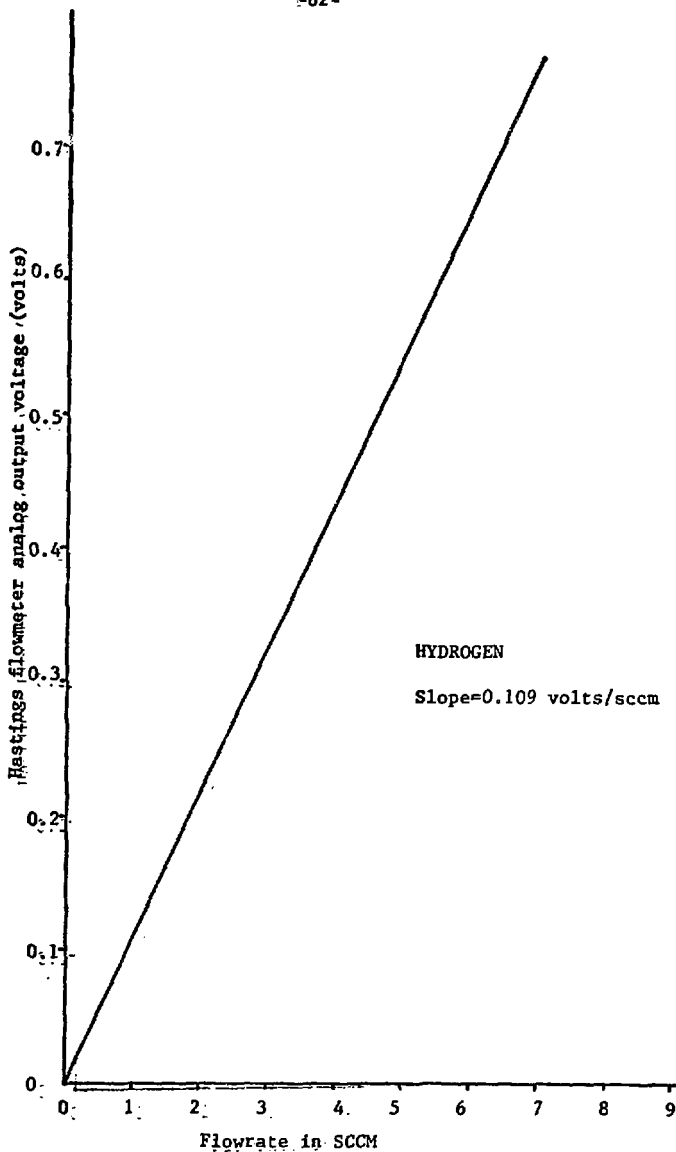
HASTINGS FLOWMETER CALIBRATION (ANALOG OUTPUT vs FLOWRATE
AS MEASURED BY THE MERCURY BUBBLE LEAK)

Fig. 33

REFERENCES

1. M. Kaminsky, S.K. Das and P. Souza. "Neutron Sputtering
    of Solids," in Advances in Chemistry Series 158,
    R.F. Gould, ed. (American Chemical Society, Washington, D.C.,
    1976).

2. M.J. Drinkwine, Y. Shapira and D. Lichtman. "Electron
    and Photon-induced Desorption," in Advances in Chemistry
    Series 158, R.F. Gould, ed. (American Chemical Society,
    Washington, D.C., 1976).

3. M. Borghi and B. Ferrario. J. Vac. Sci. Tech. 14, 570
    (1977).

4. R. Calder and G. Lewin. Brit. J. Applied Physics 18, 1459
    (1967).

5. K.H. Berkner, et al. Cryopump, Neutral-Beam Compatibility
    Test. Lawrence Berkeley Laboratory, LBL-5943 (1977).

6. H.J. Halama. AGS Division H⁻ Technical Note No. 4.
    Accelerator Division, Brookhaven National Laboratory, Upton,
    New York (1974).

7. J.T. Hogan and H.C. Howe. J. of Nuclear Materials 63, 151
    (1976).

8. T. Kammash. Fusion Reactor Physics (Ann Arbor Science,
    Ann Arbor, Mich.,1976).

9.   D.M. Meade. Nuclear Fusion 14, 289 (1974).

10.   W.J. Karzas and R. Latter. Astrophy. J. Suppl. 55 (6), 167 (1961)

11.   R.F. Post. J. Nucl. Energy 3, 273 (1961).

12.   E. Hinnov. Princeton Plasma Physics laboratory, MATT-777 (1970).

13.   D.E. Post, et al. Princeton Plasma Physics Laboratory. MATT-1262 (1976).

14.   J.P. Girard, D.A. Marty and P. Moriette. Proceedings of the First International Conference on Plasma Physics and Controlled Fusion Research (IAEA, Vienna, 1975) p. 681.

15.   D.L. Jassby. Nuclear Fusion 17 (2), 309 (1977).

16.   R. Kelly and N.Q. Lam. Rad. Effects 19, 39 (1973).

17.   W.M. Tang, P.H. Rutherford, H.P. Furth, and J.C. Adams. Phys. Rev. Lett. 35, 660 (1975).

18.   T. Ohkawa. Kakuyugo Kenkyu 32, 67 (1974).

19.   LBL/LLL CTR Staff. LBL-3296, Lawrence Berkeley Laboratory (1975).

20.   T.J. Duffy and L.D. Oddon. Lawrence Livermore Laboratory, UCRL-77236 (1975).

21.   C. Benvenuti and R.S. Calder. CERN Report, CERN-ISR-VA/69-78.

22.   T.J. Lee. Nat. Phys. Sci.231 (26), 193 (1971).

23.   C. Benvenuti, R.S. Calder and G. Pasardi. J. Vac. Sci. Tech. 13 (6), 172 (1976).

24. S.K. Erents and G.M. McCracken. J. Appl. Phys. 44 (7), 3139 (1973).

25. L.C. Pittenger. Lawrence Livermore Laboratory, UCRL-78501 (1976).

26. J. Haughian. Lawrence Berkeley Laboratory, Mechanical Engineering Note CT 0301,M4918.

27. H.M. Roder, G.E. Childs, R.D. McCarty and P.E. Augerhofer. Nat. Bur. of Stand. Tech. Note 641 (U.S. Government Printing Office, Washington, D.C. 1973).

28. C.K. Briggs, et al. Lawrence Livermore Laboratory, UCRL-76708 (1975).

29. E.E. Anderson. Modern Physics and Quantum Mechanics (W.B. Saunders, Philadelphia, PA, 1971).

30. D. McCarthy. Hydrogen Technological Survey-Thermophysical Properties, NASA Report, SP-3089 (NASA, Lewis Research Center, Washington, NASA, 1975).

31. W.J. Moore. Physical Chemistry 4th ed. (Prentice-Hall, New York, N.Y., 1973).

32. D.E. Miller. J. Chem. Phys. 42, 2089 (1965).

33. R.L. Mills and A.F. Shuck. Phys. Rev. Letters 15, 722 (1965).

34. K.F. Mucker, S. Talhouk, P.M. Harris, D. White, and R.A. Erikson. Phys. Rev. Letters 15, 586 (1965).

35. H.J.Halama, C.K. Lam and J.A. Bamberger. *J. Vac. Sci. Tech.* $\underline{14}$ (5), 1201 (1977).

36. L.E. Valby. Lawrence Livermore Laboratory, UCRL-79708 (1977).

37. A.R. Sweedler, et al. in *Radiation Effects and Tritium Technology For Fusion Reactors*. CONF-750989 (Oak Ridge National Laboratory, Tennessee, 1975).

38. M. Soell in *Eighth Symposium on Fusion Technology* (Euratom, Brussels, Belgium, 1974).

39. J.E. Faulkner, G. Gibson and J. Jedruch. Westinghouse Electric Corporation Report, WFPS-TME-022, 1975.

40. M.W. Thompson. *Defects and Radiation Damage in Metals.* (Cambridge University Press, Cambridge, 1969).

41. A. Seeger in Proceedings of the *Second United Nations International Conference on the Peaceful Uses of Atomic Energy*, Geneva, 1958, $\underline{6}$, 250 (United Nations, N.Y., 1958).

42. Reference letter dated November 24, 1967 to L. Stoller, UCB. Private communications.

43. A. Calamand. "Fission Neutron Averaged Cross-Sections" in *Handbook on Nuclear Activation Cross-Sections* (IAEA, Vienna, 1974).

44. J.R. Clemment and E.H. Quinnell. *Rev. of Sci. Instr.* $\underline{23}$ (5), 213 (1952).